THE JOURNAL OF PHYSICAL CHEMISTRY B

Article

pubs.acs.org/JPCB

Force Field Development for Actinyl Ions via Quantum Mechanical Calculations: An Approach to Account for Many Body Solvation Effects

Neeraj Rai, Surya P. Tiwari, and Edward J. Maginn*

Department of Chemical and Biomolecular Engineering, University of Notre Dame, 182 Fitzpatrick Hall, Notre Dame, Indiana 46556, United States

Supporting Information

ABSTRACT: Advances in computational algorithms and methodologies make it possible to use highly accurate quantum mechanical calculations to develop force fields (pair-wise additive intermolecular potentials) for condensed phase simulations. Despite these advances, this approach faces numerous hurdles for the case of actinyl ions, AcO_2^{n+} (high-oxidation-state actinide dioxo cations), mainly due to the complex electronic structure resulting from an interplay of s, p, d, and f valence orbitals. Traditional methods use a pair of molecules ("dimer") to generate a potential energy surface (PES) for force field parametrization based on the assumption that many body polarization effects are negligible. We show that this is a poor approximation for aqueous phase uranyl ions and present an alternative approach for the development of actinyl ion force fields that includes important many body solvation effects. Force fields are developed for the UO_2^{2+} ion with the SPC/Fw, TIP3P, TIP4P, and TIP5P water models and are validated by carrying out detailed molecular simulations on the uranyl aqua ion, one of the most characterized actinide systems. It is shown that the force fields faithfully reproduce available experimental structural data and hydration free energies. Failure to account for solvation effects when generating PES leads to overbinding between UO_2^{2+} and water, resulting in incorrect hydration free energies and coordination numbers. A detailed analysis of arrangement of water molecules in the first and second solvation shell of UO_2^{2+} is presented. The use of a simple functional form involving the sum of Lennard-Jones + Coulomb potentials makes the new force field compatible with a large number of available molecular simulation engines and common force fields.

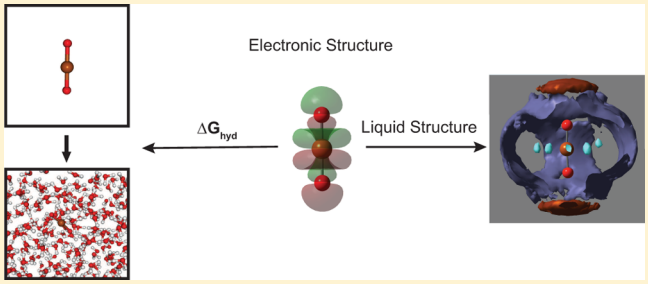

INTRODUCTION

The radiotoxicity of actinide elements presents an enormous challenge in carrying out experimental studies for their thermodynamic and structural properties. The availability of such data is central for developing better solvent extraction processes for recycling spent nuclear fuel, and for predicting migration of these radionuclides in hydrological conditions. Molecular simulations provide an alternative to experimental studies for determining thermodynamic and structural properties in the condensed phase.[1] However, the accuracy of such thermodynamic predictions depends on the ability of the force field employed to faithfully represent the true intermolecular interactions. The availability of good force fields is crucial to modeling actinide systems with high fidelity.

In an early work, Guilbaud and Wipff developed a force field for the uranyl (UO_2^{2+}) cation.[2] The force field was derived by refining parameters to match experimental uranyl structural parameters and the hydration free energy. This approach ensures that the resulting force field will model uranyl systems with good reliability. Unfortunately, fitting force fields to experimental data is not an option for other actinide elements, as experimental data suitable for force field parametrization are extremely scarce for transuranium actinides. An alternative approach for developing force fields is to use quantum mechanical calculations to generate a potential energy surface (PES) for the species of interest. For example, to generate a pairwise potential for an ion and a water molecule, the energies of different configurations of the ion/water "dimer" are computed and these energies are used to fit an analytical functional form that can be used in molecular simulations.[3−11] Using this approach, Hagberg et al.[12] developed pair potentials for the uranyl−water system. They employed multiconfigurational complete active space second-order perturbation theory[13] (CASPT2) and showed that the resulting pair potentials reproduced experimentally observed structural parameters such as water coordination number in the first solvation shell.[12] However, the density of the systems simulated by Hagberg et al.[12] was 0.477 g/cm^3, which is about half the experimental water density at ambient conditions, suggesting a deficiency in the water model employed in the study.

Although it is possible to follow this traditional approach of using a dimer to generate a PES for monovalent and divalent

Received: March 24, 2012
Revised: August 2, 2012
Published: August 2, 2012

dx.doi.org/10.1021/jp3028275 | J. Phys. Chem. B 2012, 116, 10885−10897

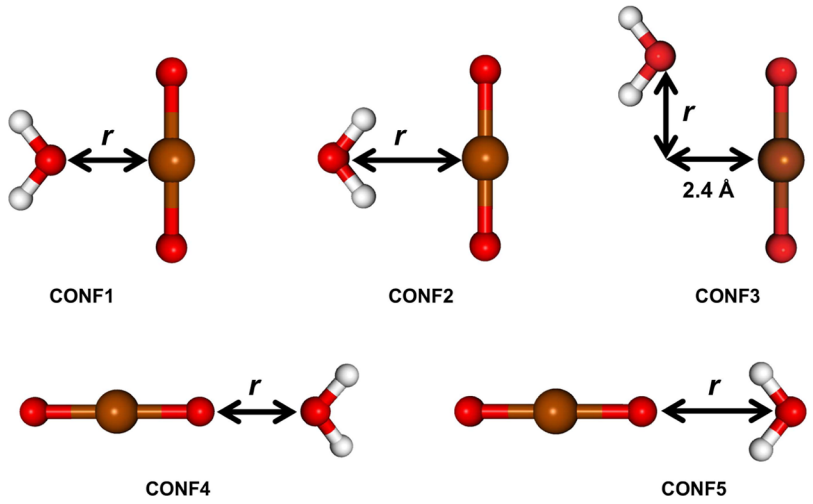

Figure 1. Configurations used to generate potential energy curves. The brown, red, and white colors represent uranium, oxygen, and hydrogen atoms, respectively.

ions interacting with neutral species such as water, there have been difficulties reported for highly charged actinide ions such as curium(III)[14] and thorium(IV),[15] or when developing potentials for two ionic species.[16] In these cases, electron transfer from one monomer (anion) to the other (cation) makes it impossible to generate a PES for correct electronic states. In the condensed phase, these ions are stabilized due to solvation effects and do not exhibit the extensive charge transfer as observed in the case of the unsolvated or "bare" ions in the gas phase. To suppress the electron transfer, one can use extra water molecules to explicitly "solvate" the ionic species while generating potential energy curves.[14−16] Hagberg et al.[14] used a single water molecule to solvate the *Cm*(III) ion when generating the *Cm*(III)/H_2O PES, while Atta-Fynn et al.[17] used six water molecules for the same system. Similarly, Réal et al.[15] employed a combination of dimer energetics and Th(IV) solvated by 10 water molecules to develop an effective pair potential for modeling hydration of Th(IV). These studies[12,14−17] focused primarily on elucidating structural properties and completely ignored thermodynamic properties such as the free energy of hydration, which is a direct indicator of whether the developed potentials capture the true interactions present in the condensed phase. The use of a different number of water molecules to prevent the electron transfer for different actinide ions makes these force fields inconsistent with each other, as they represent different PESs for ion/water interactions.

In the present study, we perform a combined quantum mechanical and molecular simulation study to establish an approach to develop force field parameters for modeling condensed phase actinyl systems. Our main goal is to determine a suitable quantum mechanical PES that should be used for force field development for actinyl ions so that the force field not only predicts correct structural properties but also the thermodynamic properties, and is internally consistent. More specifically, we want to determine if one should use the bare or the solvated ion to generate the PES. Furthermore, if it is the solvated ion PES, then what is the appropriate number of water molecules that should be used to solvate the ion? To answer these questions, we selected the uranyl−water system because it is one of the most characterized actinyl systems, and therefore serves as a basis to establish a force field development protocol for other actinyl species. Since the available benchmark experimental data are the hydration properties of uranyl ion at infinite dilution, the water model employed plays an important role. Therefore, it is important to use a well-validated water model. In addition, it is important to determine if the results depend on the water model used. For these reasons, we used four widely adopted water models, namely, SPC/Fw,[18,19] TIP3P,[20] TIP4P,[20] and TIP5P.[21]

The rest of the article is organized as follows: In the next section, we provide details of the electronic structure calculations and molecular simulations. Following this, we discuss solvation effects on the UO_2^{2+}/H_2O PES and simulation results for force fields developed based on the bare uranyl as well as the solvated uranyl PES.

COMPUTATIONAL METHODS AND SIMULATION DETAILS

All electronic structure calculations were performed with either the MolPro program suite[22] or the Gaussian 09 program suite.[23] Scalar relativistic effects were included by means of Stuttgart relativistic energy-consistent small-core pseudopotentials (ECP60MWB).[24] For uranium, the ECP60MWB associated atomic natural orbital basis set (ECP60MWB_ANO)[25] was used for MolPro calculations, while the segmented basis set (ECP60MWB_SEG)[26] was used for Gaussian calculations. The aug-cc-pVTZ[27] and aug-cc-pwCVTZ[28] basis sets were used for the hydrogen and oxygen atoms, respectively. The aug-cc-pwCVTZ basis set in the Gaussian format was downloaded from the EMSL basis set exchange,[29,30] while ECP60MWB_SEG in the Gaussian format was downloaded from the Stuttgart/Köln group basis set library.[31] All monomer geometries were minimized at the Møller−Plesset second-order perturbation (MP2) level of theory,[32] and kept rigid while generating potential energy curves. The counterpoise method due to Boys and Bernardi[33,34] was employed to correct for basis set superposition error. The configurations used for generating the PES are shown in Figure 1.

The nonbond interactions were modeled with simple Lennard-Jones (LJ) and Coulomb potentials given by

$$U(r_{ij}) = 4\varepsilon_{ij}\left[\left(\frac{\sigma_{ij}}{r_{ij}}\right)^{12} - \left(\frac{\sigma_{ij}}{r_{ij}}\right)^{6}\right] + \frac{q_i q_j}{4\pi\varepsilon_0 r_{ij}} \quad (1)$$

dx.doi.org/10.1021/jp3028275 | J. Phys. Chem. B 2012, 116, 10885−10897

where r_{ij}, σ_{ij}, ε_{ij}, q_i, q_j, and ε_0 are the separation between two interacting sites, LJ size, LJ well depth, partial atomic charge on sites i and j, and the permittivity of vacuum, respectively. The starting guess for partial atomic charges for uranyl interaction sites (uranium (UU) and apical oxygen (OU)) were computed using the Merz−Singh−Kollman (MK) approach.[35,36] Since an MK radius is not available for U, universal force field (UFF) radii[37] were used for both U and O atoms for consistency. The polarizable continuum solvation model using the integral equation formalism (IEFPCM)[38] as implemented in Gaussian 09 was used for geometry optimization and partial atomic charge determination. The solvation calculation employed the B3LYP hybrid density functional[39] and *n*-octanol as the solvent. Since the same geometrical parameters for uranyl will be used in different systems such as water (polar) and alkanes (non-polar), *n*-octanol provides a good compromise between these two extremes. The residual difference between the total quantum mechanical energy and the Coulomb energy was fit to the LJ functional form. Since the water models employed in the present study have a single LJ interaction site centered on the oxygen atom, the fitting process involved optimizing cross interactions of the UU and OU sites with the water oxygen atom (OW), and the charge on the uranium atom (q_{UU}). This resulted in five parameters to optimize: σ_{UU-OW}, ε_{UU-OW}, σ_{OU-OW}, ε_{OU-OW}, and q_{UU}. The LJ parameter space was explored via a brute force stochastic search scheme. Starting with the q_{UU} obtained from QM calculations, 20 000 sets of four cross LJ parameters were generated within a reasonable bound (2.0 Å < σ < 3.5 Å and 0.0 kcal/mol < ε < 20.0 kcal/mol) simultaneously using random numbers, and the Boltzmann weighted absolute error was computed for each set. These bounds were set based on inspection of the short-range potential being modeled by the LJ functional form. The temperature for Boltzmann weighted absolute error was set to 50 000 K for the bare uranyl case and 25 000 K for the solvated uranyl case. The results for three sets with the smallest weighted absolute error were plotted and visually inspected for a good fit. If these were not satisfactory, the charges on UU and OU were altered and the above process was repeated. The "goodness" of the fit was a combination of weighted absolute error and the ability of the fit to reproduce the global minimum position within 0.05 Å and energy with an error no more than 5 kJ/mol. The later requirement sometimes necessitated minor adjustments to the parameters obtained in the automated search process. The resulting LJ parameters and partial atomic charges are presented in Table 1.

The uranyl equilibrium bond length (1.76 Å) and bend angle (180°) were taken from the optimized geometry of the uranyl ion at the MP2 level with *n*-octanol implicit solvent. The force constants for harmonic bond stretching and bond bending terms were taken from the work of Guilbaud and Wipff.[2] Although not done in the present case, these intramolecular parameters can be obtained easily by frequency analysis on the minimized structure at a suitable level of electronic structure theory.

Monte Carlo simulations in the isobaric−isothermal (NpT) ensemble were carried out to generate trajectories for structural analysis. Simulations were carried out at T = 298.15 K and p = 101.3 kPa. The system consisted of one uranyl ion and 500 water molecules. A uniform background charge was added to make the system neutral. A radial cutoff of 10 Å with analytic long-range corrections[40] was used to compute the LJ potential. The Ewald summation method with tin foil boundary conditions was used to compute long-range Coulombic interactions.[40−42] A radial cutoff of r_{cut} = 10 Å was used for the real space part of the Ewald summation. The Ewald sum convergence parameter, α, was set to $3.2/r_{cut}$, while the reciprocal space cutoff, k_{cut}, was set to $2.0 \times \pi \times \alpha$.

Table 1. The Non-Bond Interaction Parameters Developed in This Work[a]

	Bare Uranyl			
	SPC/Fw	TIP3P	TIP4P	TIP5P
q_{UU} (e)	3.08	3.08	3.08	3.08
q_{OU} (e)	−0.54	−0.54	−0.54	−0.54
σ_{UU-OW} (Å)	2.32	2.35	2.31	2.37
σ_{OU-OW} (Å)	2.39	2.49	2.24	2.50
ε_{UU-OW} (kJ/mol)	21.92	16.32	21.92	19.00
ε_{OU-OW} (kJ/mol)	2.72	0.84	8.08	1.72
	Solvated Uranyl (Recommended for Use)			
	SPC/Fw	TIP3P	TIP4P	TIP5P
q_{UU} (e)	2.50	2.50	2.50	2.50
q_{OU} (e)	−0.25	−0.25	−0.25	−0.25
σ_{UU-OW} (Å)	3.25	3.25	2.78	3.26
σ_{OU-OW} (Å)	3.00	3.00	3.07	2.92
ε_{UU-OW} (kJ/mol)	0.27	0.27	1.39	0.26
ε_{OU-OW} (kJ/mol)	1.08	1.08	0.85	1.47

[a]The bare uranyl parameters are presented here for completeness sake and should not be used. The solvated uranyl parameters are recommended for use.

During the production runs, translations of center of mass, rotations, configurational-bias regrowth moves, and volume moves were attempted with 40, 40, 19.5, and 0.5% probabilities, respectively. The configurational-bias growth moves used the dual cutoff scheme proposed by Vlugt et al.[43] For flexible models (uranyl and SPC/Fw), MC simulations used fixed bond lengths while bond angles were sampled by carrying out a pre-simulation of fragments populating a reservoir of fragment conformations used during configurational-bias moves.[44,45] The production runs consisted of 8×10^5 MC cycles (1 MC cycle consisted of 501 moves). The trajectories were stored every 5 MC cycles for structural analysis. Monte Carlo simulations and structural analysis were carried out by the simulation suite CASSANDRA developed in our group. Figure 2 is a schematic representation of the molecular frame of reference used for spatial distribution functions (SDFs), water dipole moment vector, the plane normal, and the definition of apical and

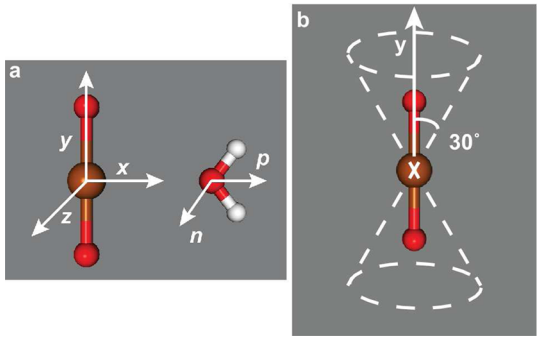

Figure 2. (a) Schematic representation of the molecular frame of reference used for spatial distribution functions, and water dipole (**p**) and water plane normal (**n**) vectors. (b) Definition of the apical conical region used in structural analysis.

dx.doi.org/10.1021/jp3028275 | J. Phys. Chem. B 2012, 116, 10885−10897

Table 2. Calculation of Hydration Free Energies for Uranyl Ion

	Solvation Free Energy (kJ/mol)						
system	ΔG_{hyd}^{Coul}	ΔG_{hyd}^{LJ}	ΔG_{hyd}^{sim}	ΔG_{corr}^{surf}	$\Delta G_{corr}^{ion-ion}$	$\Delta G_{corr}^{ion-solvent}$	ΔG_{hyd}[a]
				Bare Uranyl			
SPC/Fw	−1846.49	−181.06	−2027.55	−108.51	−1.86	1.93	−2128
TIP3P	−1839.82	−104.52	−1944.34	−101.24	−1.47	1.89	−2037
TIP4P	−1726.81	−255.33	−1982.14	−98.95	−2.50	1.89	−2074
TIP5P	−1961.24	−144.25	−2105.49	−18.21	−1.66	1.89	−2116
				Solvated Uranyl			
SPC/Fw	−1336.9	5.21	−1331.69	−108.51	−1.86	1.93	−1432
TIP3P	−1324.66	4.70	−1319.96	−101.24	−1.47	1.89	−1413
TIP4P	−1293.51	1.02	−1292.49	−98.95	−2.50	1.89	−1384
TIP5P	−1463.19	−3.43	−1466.62	−18.21	−1.66	1.89	−1477
Expt.[b]							−1665 ± 65
Expt.[c]							−1360 ± 24

[a] ΔG_{hyd} includes correction for different experimental and simulation reference states (7.92 kJ/mol). The uncertainty in the reported numbers is approximately 1 kJ/mol. [b] Using Gibson et al. data.[78] [c] Using Marcus data.[72]

equatorial regions. When the uranyl ion is nonlinear, the x axis is defined as the OU−UU−OU angle bisector projected along one of the UU−OW vectors for water in the first solvation shell, the z axis is normal to the x axis and the UU−OU bond vector, and the y axis is the cross product between the x and z axes. The apical region of uranyl is defined as a region within a cone with axis along the UU−OU bond vector and 30° angle with the cone axis. The region outside this cone is referred to as the equatorial region. The SDFs were visualized in GaussView, version 5.[46]

Gibbs hydration free energies were calculated using molecular dynamics simulations using GROMACS-4.5.5[47,48] and Bennett's acceptance ratio (BAR) method[49] as implemented in the g_bar tool available in the GROMACS-4.5.5 suite. The hydration free energy of the ion (ΔG_{hyd}^{sim}) was calculated along a path that couples a noninteracting ion in the bulk solvent to a fully solvated ion in the bulk solvent. This simulation path was split into two steps: growth and charging.[50] First, ion−water LJ interactions were coupled along path coordinate λ_{LJ} to get the LJ contribution to the free energy (ΔG_{hyd}^{LJ}). Following this, ion−water Coulombic interactions were coupled along λ_{Coul} to get the Coulombic contribution to the free energy (ΔG_{hyd}^{Coul}). Thus, ΔG_{hyd}^{sim} is the sum of ΔG_{hyd}^{LJ} and ΔG_{hyd}^{Coul}. We used 21 equally spaced steps each for λ_{LJ} and λ_{Coul} to get the final coupled ion in the bulk solvent.

The system consisted of 5000 water molecules and a single uranyl ion in a cubic box with 53.4 Å edge lengths. Such a large system size was chosen to minimize the finite size corrections to be applied to ΔG_{hyd}^{sim} due to the periodicity . The geometries of water molecules for the rigid TIP3P, TIP4P, and TIP5P water models were constrained using the SETTLE algorithm.[51] A switch function was used for the LJ interactions to shift the LJ force starting from 10 Å to make it zero at a cutoff distance of 12 Å. Periodic boundary conditions were applied in all three directions, and the particle-mesh Ewald[52,53] (PME) method with tin foil boundary conditions was used to handle long-range electrostatic forces. MD simulations were performed with a time step of 2 fs except in the case of the flexible water (SPC/Fw) system, where a time step of 1 fs was used. A Langevin stochastic dynamics (SD) algorithm[54] was used for integrating the equations of motion. Long-range dispersion corrections were applied for energy and pressure. Energy minimization followed by 100 ps of simulation in the canonical ensemble (NVT) followed by 500 ps of simulation in the NpT ensemble was used to equilibrate the system. Final data collection simulations for free energy calculations were carried out for 5 ns in the NpT ensemble at a temperature of 298.15 K and a pressure of 101.3 kPa. This was done for each $\lambda \in \{0, 0.05, 0.1, 0.15, ..., 0.95, 1\}$ for both λ_{LJ} and λ_{Coul}; thus, a total of 42 × 5 ns of data collection was done. Temperature coupling was done implicitly while using the SD algorithm, and pressure coupling was done using the Parrinello−Rahman method.[55,56] The length of equilibration and data collection simulation runs are much larger than the previously reported hydration free energy simulations[57,58] to ensure good statistical precision. The statistical uncertainties in the computed hydration free energies were determined by using the block averaging method, and were found to be smaller than 1 kJ/mol. The details of the soft core potential used are provided in the Supporting Information.

The absolute hydration free energy of an ion (ΔG_{hyd}) is calculated by adding correction terms to the hydration free energy (ΔG_{hyd}^{sim}) obtained from simulation[58]

$$\Delta G_{hyd} = \Delta G_{hyd}^{sim} + \Delta G_{corr}^{ion-ion} + \Delta G_{corr}^{ion-solvent} + \Delta G_{corr}^{press} + \Delta G_{corr}^{surf} \quad (2)$$

In this expression, $\Delta G_{corr}^{ion-ion}$ is the ion−ion correction term, which accounts for artifacts arising from interactions between an ion and its periodic images in the Ewald summation.[58−61] $\Delta G_{corr}^{ion-solvent}$ is the ion−solvent correction term, which accounts for inappropriate orientational polarization of the solvent due to interactions between periodic images of the ion and nearby solvent molecules.[57−62] The last two terms in eq 2 are added to enable direct comparison with experiment. ΔG_{hyd}^{press} is the pressure correction term due to the difference in the ideal gas standard state between simulation and experiment.[57,58,61] ΔG_{hyd}^{surf} is the correction due to the surface potential of the vacuum/water interface.[57,58] Details of the surface potential calculation are provided in the Supporting Information. A more detailed explanation of these correction terms can be found elsewhere.[57,58] Note that, for $\Delta G_{corr}^{ion-solvent}$, a conservative radius of 5 Å was used for the cavity. Although the correction terms $\Delta G_{corr}^{ion-ion}$ and $\Delta G_{corr}^{ion-solvent}$ strictly apply to point charges/spherical ions, the asphericity of the uranyl ion will have a very small effect on the results, especially given that these terms are

dx.doi.org/10.1021/jp3028275 | J. Phys. Chem. B 2012, 116, 10885−10897

approximately 0.2% of the total hydration free energy (see Table 2).

RESULTS AND DISCUSSION

We performed exploratory calculations of the UO_2^{2+}/H_2O PES for the configuration shown in Figure 3 using MP2,[32] B3LYP,[39]

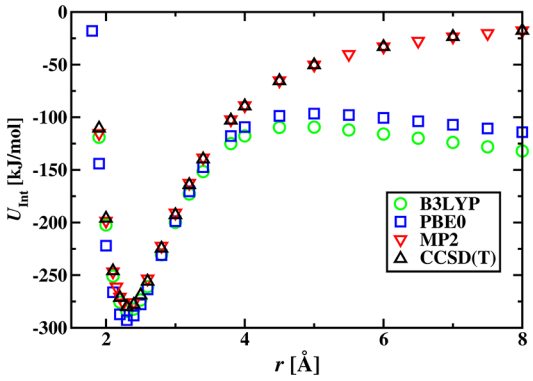

Figure 3. Potential energy curves for UO_2^{2+}/H_2O for CONF1 shown in Figure 1 using different theoretical approaches.

and PBE0[63] levels of theory to test their suitability for accurate energetics by comparing them with the benchmark energies obtained using the highly accurate CCSD(T) level of theory.[64] We found that the MP2 level yielded potential energies that were essentially identical to those obtained at the CCSD(T) level of theory (see Figure 3) but at a fraction of the computational cost. B3LYP and PBE0 functionals are in very good agreement with CCSD(T) results for short monomer separations (<3.5 Å), but for distances greater than 3.5 Å, they exhibit peculiar behavior characteristic of incorrect asymptotic behavior of the exchange correlation functional employed.[65] On the basis of these calculations, we decided to use the MP2 level of theory in the present study.

We explored the effect of solvating the uranyl ion on the UO_2^{2+}/H_2O PES by sequentially adding water molecules in the first and second solvation shells, and computing potential energy curves for different water−uranyl configurations. In the first solvation shell, water molecules were placed in the equatorial plane containing the uranium atom with water oxygen atoms at a distance of 2.32 Å from the uranium atom (the global minimum for CONF1) with the water dipole pointing away from the uranyl ion (see CONF1 in Figure 1), and along the uranyl molecular axis 2.4 Å from the uranyl oxygen. In the second solvation shell, water molecules were placed in the equatorial plane at 4.32 Å from the uranium atom. These configurations are provided in xyz format in the Supporting Information. The interaction energy (U_{Int}) of water with uranyl solvated by X water (XW) molecules is calculated according to the following relation

$$U_{Int} = \{E[UO_2^{2+}\cdot X\mathrm{W} + H_2O] - E[UO_2^{2+}\cdot X\mathrm{W}] - E[H_2O]\} - \{E[X\mathrm{W} + H_2O] - E[X\mathrm{W}] - E[H_2O]\} \quad (3)$$

where $E[Y]$ represents the MP2 energy of species Y computed with all the basis functions. In the case of $X = 0$, we retrieve the expression for the U_{Int} value of the bare uranyl ion with a single water molecule (the so-called "bare" potential).

Figure 4 depicts the UO_2^{2+}/H_2O CONF1 potential energy curve for the uranyl ion solvated by 0, 1, 3, 5, 6, and 8 water

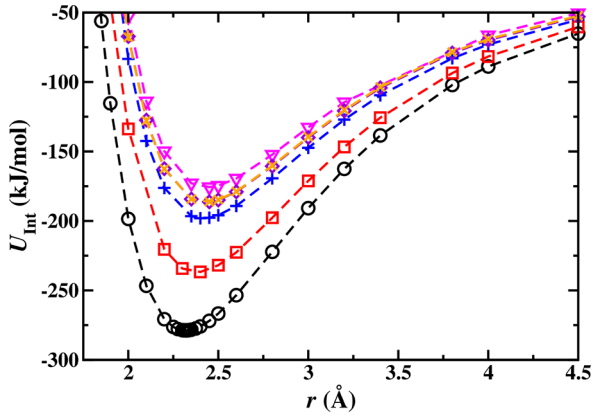

Figure 4. Effect of solvating water molecules on the potential energy curve for UO_2^{2+}/H_2O dissociation. The black circles, red squares, blue pluses, violet diamonds, orange crosses, and magenta down triangles represent data for uranyl ion solvated by 0, 1, 3, 5, 6, and 8 water molecules. The dashed lines of corresponding colors are guides to the eye.

molecules. One immediately notices that there is a sharp decrease in the magnitude of the interaction energy (~15%) upon solvating the uranyl ion with a single water molecule. This suggests that there is significant charge transfer from water to the uranyl ion, which results in a smaller effective charge on the uranyl ion. In other words, the 2+ charge on the uranyl ion is now much more delocalized, which in turn results in a "weaker" interaction between the solvated uranyl dication and the "dipolar" water molecule. Upon solvating the uranyl ion with 3 water molecules in the equatorial plane in the first solvation shell, the interaction energy decreases by approximately 30% compared to the bare uranyl case. The addition of more water molecules along the molecular axis in the apical region and in the second solvation shell has a smaller effect on the binding energy. The effect of solvation on the PES is substantial and highlights the key challenge for developing "effective" pair potentials for condensed phase simulations via quantum mechanical calculations. Should one use "bare" uranyl as done in the traditional approach or use the ion solvated by some number of water molecules, as is often necessary to suppress the electron transfer? If the latter, how many water molecules X are needed?

To answer these questions, PESs were generated for the X = 0 case and for the uranyl ion explicitly solvated by water. On the basis of results shown in Figure 4, a total of three water molecules were added to the equatorial plane for the potential energy scans of CONF1, CONF2, and CONF3, and a fourth water molecule was added for the CONF4 and CONF5 scans. Thus, effectively four water molecules in the equatorial plane (for CONF1, CONF2, and CONF3, the fourth water molecule is the water used for the potential scan) were used for all configurations. This number of water molecules was selected for the "solvated" ion PES because the addition of more water molecules has a modest effect on the energy, while, for fewer water molecules, the energy differences change significantly upon addition or removal of one water molecule. As shown below, condensed phase simulations using the "solvated" force field do an excellent job reproducing experimental thermodynamic and structural properties.

dx.doi.org/10.1021/jp3028275 | J. Phys. Chem. B 2012, 116, 10885−10897

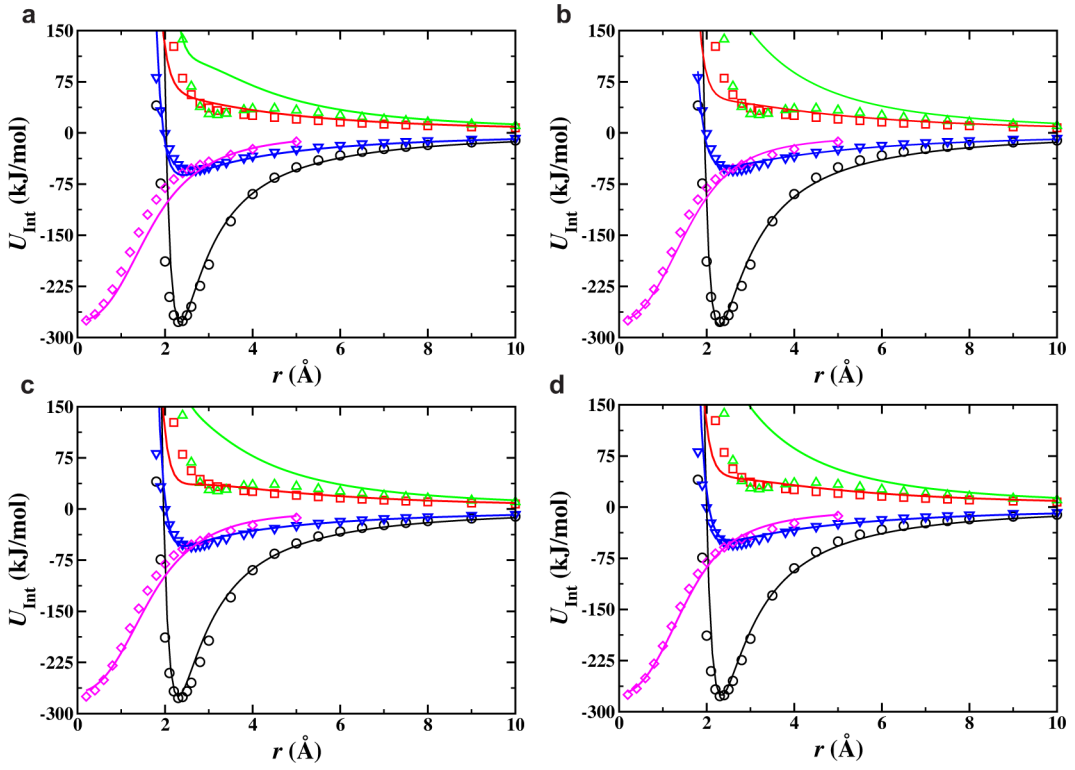

Figure 5. Potential energy curves for different unsolvated uranyl ion configurations (see Figure 1) along with fits to the sum of LJ and Coulomb potentials for different water models: (a) SPC/Fw; (b) TIP3P; (c) TIP4P; (d) TIP5P. The black circles, green up triangles, magenta diamonds, blue down triangles, and red squares represent MP2 data for CONF1, CONF2, CONF3, CONF4, and CONF5, respectively. The solid lines of the corresponding colors are fits to the sum of LJ and Coulomb potentials.

Bare Uranyl. We carried out MP2 calculations for five different configurations shown schematically in Figure 1 to generate potential energy curves. As all of the configurations except CONF5 (C_s) have C_{2v} point group symmetry, this results in significant time savings for the quantum calculations. This approach also ensures that energetically favorable configurations (CONF1, CONF3, and CONF4) are sampled adequately. Figure 5 shows the potential energy curves for each of the water models and for all five different UO_2^{2+}/H_2O configurations, along with fits to the analytical functional form. The global minimum in the potential energy surface is for the configuration labeled CONF1 at 2.32 Å with a binding energy of 279 kJ/mol. This compares well with the CASPT2 calculations by Hagberg et al.[12] who reported a binding energy of 270 kJ/mol at 2.33 Å. This suggests that second-order perturbation theory based on a single reference wave function as employed in the present study is adequate for capturing the energetics of the uranyl/water system. Hagberg et al.[12] have reported that for the same system one needs an attractive exponentially decaying charge transfer term in order to fit the quantum mechanical energy surfaces. In contrast, we find that a simple functional form which is a sum of LJ and Coulomb potential is sufficient. This is important because this type of simple potential model is used widely in molecular modeling packages, and hence can be easily used.

Figure 5 indicates that the fits are equally good for all four different water models and for all of the configurations except CONF2. For this configuration, where the water dipole moment points toward the positively charged uranyl ion, the fits are significantly more repulsive than the quantum mechanical results. In the quantum mechanical calculations, the strongly charged uranyl ion is able to significantly polarize the water molecule at small intermolecular separations (r < 5.0 Å) which reduces the dipole moment of the water molecule. This in turn results in lower repulsion between the uranyl ion and water molecule. Since a fixed charge model is used to fit the PES, it is almost impossible to capture this effect. Although the fit for CONF2 at short separations is not very accurate, it will have a negligible effect on condensed phase simulations because CONF2 is almost 300 kJ/mol higher in energy compared to CONF1 for the same uranyl water separation. In other words, for the range of temperatures relevant for physical systems (300−600 K), the probability of observing the CONF2 configurations where the fit is poor is negligible.

Monte Carlo simulations for uranyl aqua ion were carried out for each water model using the fitted potentials. Radial distribution functions (RDFs) and number integrals (NI) for UU−OW interaction sites for all the water models are shown in Figure 6. The position of the first peak in the RDFs is at 2.41, 2.41, 2.43, and 2.44 Å for SPC/Fw, TIP3P, TIP4P, and TIP5P, respectively. The second solvation shell is split into two peaks for all but the TIP5P water model. One can integrate the RDF to obtain an average number of water molecules around the uranyl ion as a function of radial distance. The bare uranyl potential yields a total of 8 water molecules in the first solvation shell for all the water models. Further analysis shows that the first shell splits into two layers above and below the equatorial plane, each containing four water molecules on the vertices of squares staggered by 45° (see Figure 1 in the Supporting Information). Although the position of the first peak agrees well with the experimental results,[66−70] the water coordination

dx.doi.org/10.1021/jp3028275 | J. Phys. Chem. B 2012, 116, 10885−10897

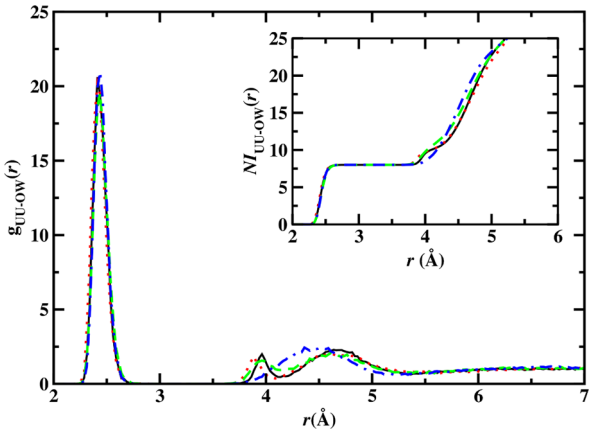

Figure 6. Radial distribution function for uranium and water oxygen ($g_{UU-OW}(r)$). The inset shows the corresponding number integrals ($NI_{UU-OW}(r)$). The solid black, dotted red, dashed green, and dash dotted blue lines represent the SPC/Fw, TIP3P, TIP4P, and TIP5P water models, respectively.

number in the first solvation is much higher than the experimentally reported value (~5).[66−71]

Direct evidence of this overestimation can be obtained by computing uranyl hydration free energies ($\Delta G_{hyd}[UO_2^{2+}]$). Before presenting results of uranyl hydration free energies, a brief discussion on the available experimental data on the free energy of hydration is presented in order to understand sources of discrepancy among different reported $\Delta G_{hyd}[UO_2^{2+}]$, and values used by researchers for comparison purposes.[2,72−77] The free energy of hydration is given by

$$\Delta G_{hyd}[UO_2^{2+}] = \Delta H_{hyd}[UO_2^{2+}] - T\Delta S_{hyd}[UO_2^{2+}] \quad (4)$$

where $\Delta H_{hyd}[UO_2^{2+}]$, T, and $\Delta S_{hyd}[UO_2^{2+}]$ are the enthalpy of hydration, temperature, and the entropy of hydration, respectively. Determination of $\Delta H_{hyd}[UO_2^{2+}]$ requires knowledge of the enthalpy of formation of $[H^+]$ ($\Delta H_f[H^+]$) and the enthalpy of hydration of $[H^+]$ ($\Delta H_{hyd}[H^+]$) according to the following relation[72,78]

$$\Delta H_{hyd}[UO_2^{2+}] = \Delta H_f[UO_2^{2+}(aq)] - \Delta H_f[UO_2^{2+}(g)] + 2(\Delta H_f[H^+(g)] + \Delta H_{hyd}[H^+(aq)]) \quad (5)$$

In the above relations, all the thermodynamic quantities are defined with respect to a suitable reference state. For the gas phase, this is an ideal gas at p = 1 bar and T = 298.15 K. For the aqueous phase, the reference state is a 1 M solution at the same T and p. From eq 5, it is evident that the proton hydration enthalpy sets the absolute scale for $\Delta H_{hyd}[UO_2^{2+}]$. The majority of the reported data[72−74,78] on uranyl hydration use the value from Halliwell and Nyburg[79] of $\Delta H_{hyd}[H^+] = -1091 \pm 10$ kJ/mol. Recently, Tissandier et al.[80] and Tuttle et al.[81] have estimated $\Delta H_{hyd}[H^+] = -1150.1 \pm 1.5$ and -1149.9 ± 1.5 kJ/mol, respectively. Although Camaioni and Schwerdtfeger[82] recommend the Tissandier et al. value as the new benchmark, others are less enthusiastic about it mainly due to the possibility of inclusion of finite size effects in the cluster-pair approximation, as they extrapolate results based on just six water molecules (for a detailed discussion, see refs 83 and 84). From the application point of view, however, differences in the solvation free energies are the important quantities. Therefore, as long as one is consistent in using particular reference values

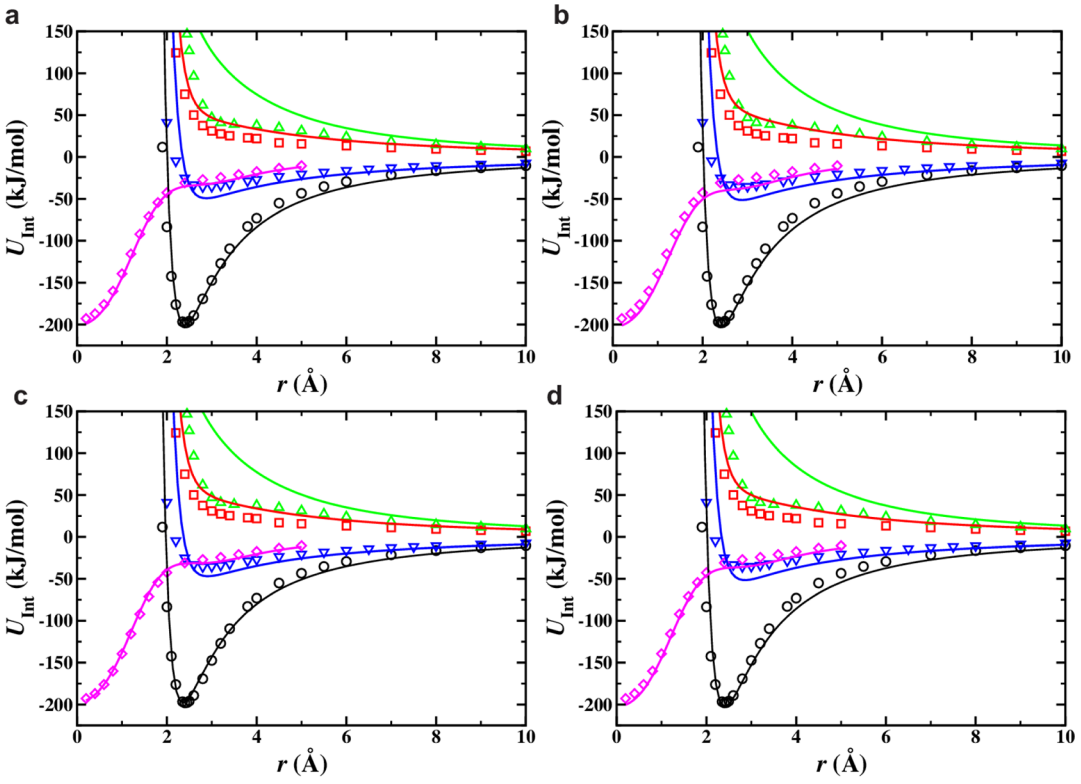

Figure 7. Potential energy curves for solvated uranyl ion along with fits to the sum of LJ and Coulomb potentials for different water models: (a) SPC/Fw; (b) TIP3P; (c) TIP4P; (d) TIP5P. The symbols and color scheme are the same as those in Figure 5.

dx.doi.org/10.1021/jp3028275 | J. Phys. Chem. B 2012, 116, 10885−10897

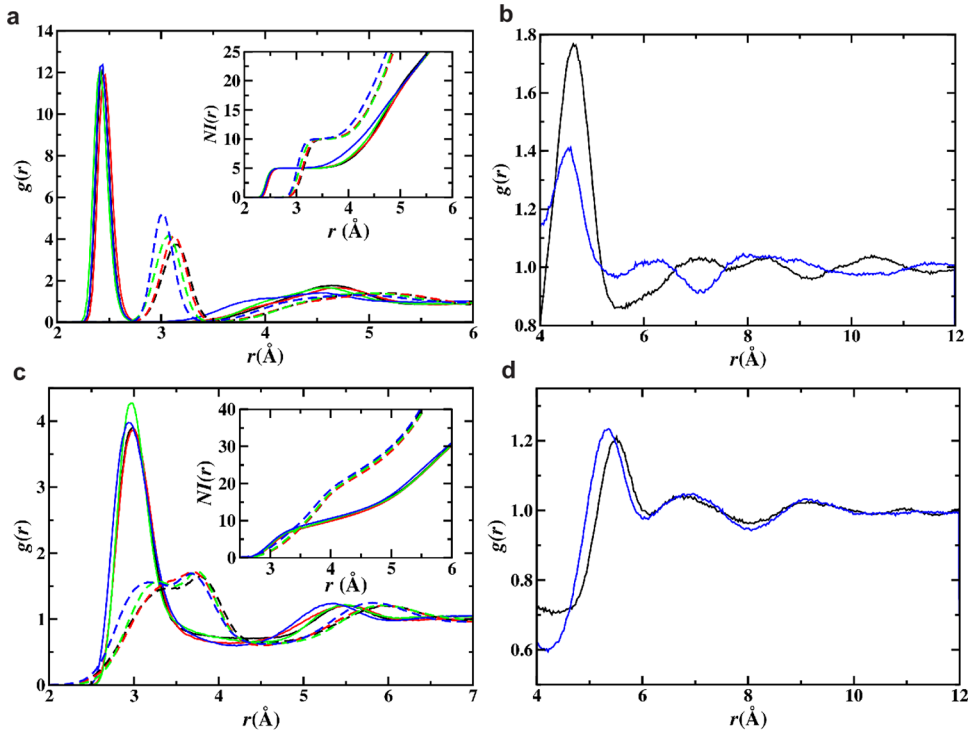

Figure 8. Radial distribution function and number integrals (inset) from simulations based on the potential developed for solvated uranyl: (a) RDF and NI for oxygen (OW) and hydrogen (HW) sites in water with uranium (UU); (b) extended RDF for UU−OW for the SPC/Fw and TIP5P water models; (c) RDF and NI for OW and HW sites with uranyl oxygen (OU); (d) extended RDF for OU−OW for SPC/FW and TIP5P models. The black, red, green, and blue colors represent the SPC/Fw, TIP3P, TIP4P, and TIP5P water models, respectively. The solid and dashed lines represent data involving OW and HW sites, respectively.

when developing force fields, choosing one reference versus another is not a cause for concern.[85] For consistency with the cited literature, we use the $\Delta H_{hyd}[H^+]$ value from Halliwell and Nyburg[79] for the discussion in the following paragraph but adopt the $\Delta H_{hyd}[H^+]$ value from Tissandier et al. for the rest of the article.

The literature on UO_2^{2+} hydration free energies is confusing and contains several subtleties that make quantitative comparison difficult. Below is a brief survey of the values that have been reported in the literature. On the basis of the lattice energy of the UO_2F_2 crystal,[72] Marcus recommends the following values: $\Delta H_{hyd}[UO_2^{2+}] = -1363 \pm 23$ kJ/mol, $\Delta S_{hyd}[UO_2^{2+}] = -403 \pm 3$ J mol^{-1} K^{-1}, and $\Delta G_{hyd}[UO_2^{2+}] = -1243 \pm 24$ kJ/mol.[74] Since the work of Marcus, Cornehl et al.[86] and Gibson et al.[78] have reported gas phase enthalpies of formation of $\Delta H_f[UO_2^{2+}] = -1552 \pm 251$ and -1524 ± 63 kJ/mol, respectively. Using Gibson et al.'s value of $\Delta H_f[UO_2^{2+}]$, one obtains $\Delta H_{hyd}[UO_2^{2+}] = -1665 \pm 64$ kJ/mol.[78] Shamov and Schreckenbach[75] and Gutowski and Dixon[77] used Gibson et al.'s $\Delta H_{hyd}[UO_2^{2+}]$ value but an erroneous value of $\Delta S_{hyd}[UO_2^{2+}] = -329$ J mol^{-1} K^{-1} from Marcus[72] to compute $\Delta G_{hyd}[UO_2^{2+}]$. They reported $\Delta G_{hyd}[UO_2^{2+}] = -1761$ kJ/mol instead of −1567 kJ/mol due to an algebraic mistake.[76] Using a more reliable value for $\Delta S_{hyd}[UO_2^{2+}]$[74] ($-403 \pm 3$ J mol^{-1} K^{-1}), one finds that $\Delta G_{hyd}[UO_2^{2+}] = -1545 \pm 65$ and -1665 ± 65 kJ/mol with the Halliwell and Nyburg[79] and Tissandier et al.[80] absolute proton hydration enthalpies, respectively.

It is therefore not possible to cite a "correct" absolute hydration free energy; instead, we take the value of -1360 ± 24 kJ/mol from Marcus[72] as the upper bound and the value of -1665 ± 65 kJ/mol from Gibson et al.[78] with the proton hydration enthalpy of Tissandier et al.[80] as the lower bound. At the very least, a good force field should give computed hydration free energies within this range.

In Table 2, we present $\Delta G_{hyd}[UO_2^{2+}]$ at $T = 298.15$ K and $p = 101.3$ kPa for the four different water models. Using the bare uranyl force field, the computed ΔG_{hyd} have values of −2128, −2037, −2074, and −2116 kJ/mol for SPC/Fw, TIP3P, TIP4P, and TIP5P, respectively. The ΔG_{hyd} for all the water models considered are significantly below the lower bound of -1665 ± 65 kJ/mol. The TIP5P water model underestimates $\Delta G_{hyd}[UO_2^{2+}]$ by approximately 27%, while the TIP3P model underestimates it by approximately 22%. The SPC/Fw and TIP4P models fall between these two extremes. This, combined with the fact that the coordination numbers are too high, suggests that the interaction strength between water and the uranyl ion is severely overestimated when using "bare" uranyl interaction energies. This force field, obtained by ignoring the many body solvation effects, therefore does not represent the true "effective" pair potential suitable for modeling condensed phase systems.

Solvated Uranyl. The potential energy scans for different solvated configurations and fits to the sum of LJ and Coulomb potential for different water models are shown in Figure 7. The overall quality of the fits is almost as good as that of the bare uranyl case. The main difference is between the bare and the solvated uranyl fit for CONF3, where the fitted potential overestimates the strength of the interaction energy. This is mainly because we maintain an overall charge of 2+ on the uranyl cation while fitting, despite indications of significant charge transfer (~0.4|e|) from water molecules to the uranyl ion. This was estimated from calculations of the partial atomic charges derived from the electrostatic potential for the penta-aquo uranyl complex in *n*-octanol implicit solvent. This is

dx.doi.org/10.1021/jp3028275 | J. Phys. Chem. B 2012, 116, 10885−10897

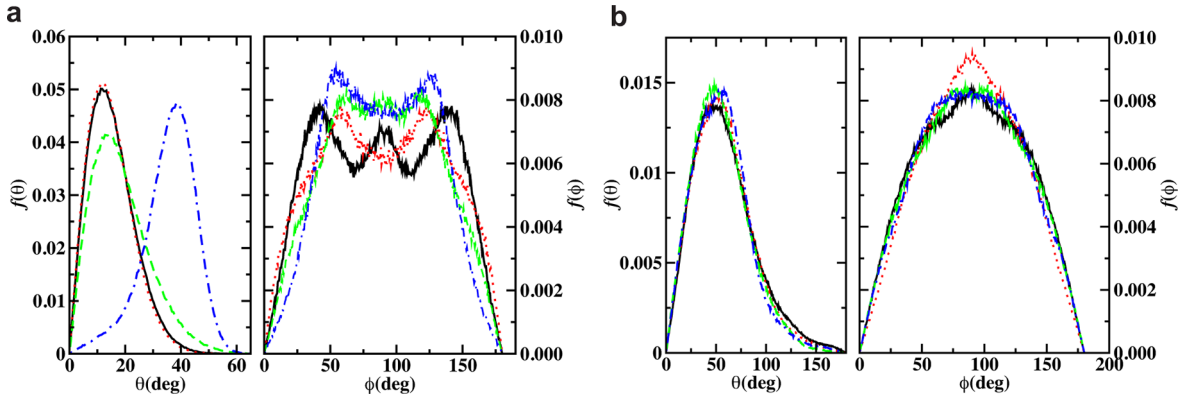

Figure 9. Distribution of the angle between the water dipole moment and UU−OW vector (θ) and the water plane normal and UU−OU vector (ϕ). Parts a and b show the data for the first and second solvation shells, respectively, in the UU−OW RDF. The solid black, dotted red, dashed green, and dash-dotted blue colors represent data for SPC/Fw, TIP3P, TIP4P, and TIP5P, respectively.

somewhat smaller than 0.78|e| obtained by Hemmingsen et al.[87] using Mulliken population analysis. In a related work, Clavaguéra-Sarrio et al. have performed extensive work on determining the contribution of charge transfer to total interaction energy.[88] This effect could be captured by adding polarizability to the potential,[12] explicitly adding charge transfer terms,[88] or by reducing the net charge on the uranyl ion. We chose not to do this, however, because we are most interested in developing a simple and fast fixed charge model. We imposed the constraint that the uranyl ion had to have a charge of 2+ to facilitate its use with counterions having integer charges. These approximations are justified given that the error introduced due to the overestimation of interaction energy is expected to be smaller than the 65 kJ/mol error bars on the experimental hydration free energy.

The hydration free energies for the force fields derived from solvated uranyl are presented in Table 2. ΔG_{hyd} are −1432, −1413, −1384, and −1477 kJ/mol for SPC/Fw, TIP3P, TIP4P, and TIP5P, respectively. The uncertainties in the computed ΔG_{hyd} are approximately 1 kJ/mol. Although the computed hydration free energies differ by as much as 140 kJ/mol, the difference after addition of correction terms mainly due to the surface potential narrows down to 90 kJ/mol. The hydration free energies of all the water models fall in the acceptable range of −1360 and −1665 kJ/mol.

Next, we look at the first solvation shell of uranyl ion for which reliable experimental data is available. The position of the first peak in the RDF for the UU−OW interaction pair is at 2.44, 2.45, 2.41, and 2.41 Å for SPC/Fw, TIP3P, TIP4P, and TIP5P, respectively (see Figure 8). These match well with the experimental estimates of 2.40−2.42 Å from extended X-ray absorption fine structure (EXAFS)[68,69,89−91] and high energy X-ray scattering (HEXS) experiments.[70,92] From UU−OW number integrals in Figure 8, it is evident that, irrespective of the water models employed, there are five water molecules in the first equatorial solvation shell, which agrees well with other experiments.[68−71,89−91]

These results show that including four water molecules to solvate the uranyl ion when generating the PES not only reproduces correct hydration free energies but also predicts the liquid structure of uranyl aqua ion consistent with the available experimental data. Thus, the resulting force field captures the "effective" interaction of the uranyl ion with a water molecule in the aqueous medium. In the next section, we present detailed structural analysis of the uranyl aqua ion.

Structure of Uranyl Aqua Ion. RDFs and NIs for UU−OW, UU−HW, OU−OW, and OU−HW interaction sites for all the water models are shown in Figure 8. The predicted first peak positions in UU−OW RDFs for all four water models (2.41−2.45 Å) agree with other computational studies.[93−95] Nichols et al.[93] carried out Car−Parrinello molecular dynamics (CPMD) using the PBE96 exchange correlation functional and found the first peak position to be 2.44−2.46 Å, while Frick et al.[94] found a slightly larger value (2.49 Å) using Hartree−Fock level quantum mechanical charge field molecular dynamics where two solvation shells were included in the quantum region. Guilbaud and Wipff[95] found the first maximum in RDF at 2.50 Å. The first peak in UU−HW RDF is approximately 0.6 Å further out than the UU−OW peak position, suggesting that first equatorial solvation shell water molecules have hydrogen atoms pointing away from the uranium atom.

The first peak in the OU−OW RDF is centered at approximately 3.0 Å for all of the models, while the first peak in the OU−HW RDF is split into two peaks with the dominant peak at 3.7 Å. The RDFs centered around apical oxygen include water molecules in the "traditional" first solvation shell of the uranyl ion equatorial plane, and the "non-traditional" first solvation shell in the apical region, as well as the second UU−OW solvation shell. Borrowing the terminology from Martínez et al.,[96] we will refer to the apical first solvation shell as the meso shell. The splitting in the first peak in the OU−HW RDF is mainly due to the highly ordered water molecules in the first solvation shell where one of the hydrogen molecules is closer to the apical oxygen than the other hydrogen atom of the same water molecule.

The peak corresponding to the second solvation shell is rather broad for all the water models (Figure 8). The second UU−OW solvation shell spans from approximately 3.5 to 5.2 Å. The maximum in the second peak is located at 4.7 Å for the TIP3P water model while at approximately 4.6 Å for other water models. The observed peak positions for different water models match well with the HEXS (4.5 Å)[92] and X-ray diffraction (4.4 Å)[66] experiments. The second solvation shell consists of about 16 water molecules. Similar coordination numbers (14−16) are reported by Nichols et al.[93] There is a large variance in the number of water molecules in the second solvation shell observed by different experimental techniques. Aberg et al.[66] used X-ray diffraction and reported the second shell coordination number to be 14, while Soderholm et al.[92] report 10 water molecules. Our simulations along with CPMD

dx.doi.org/10.1021/jp3028275 | J. Phys. Chem. B 2012, 116, 10885−10897

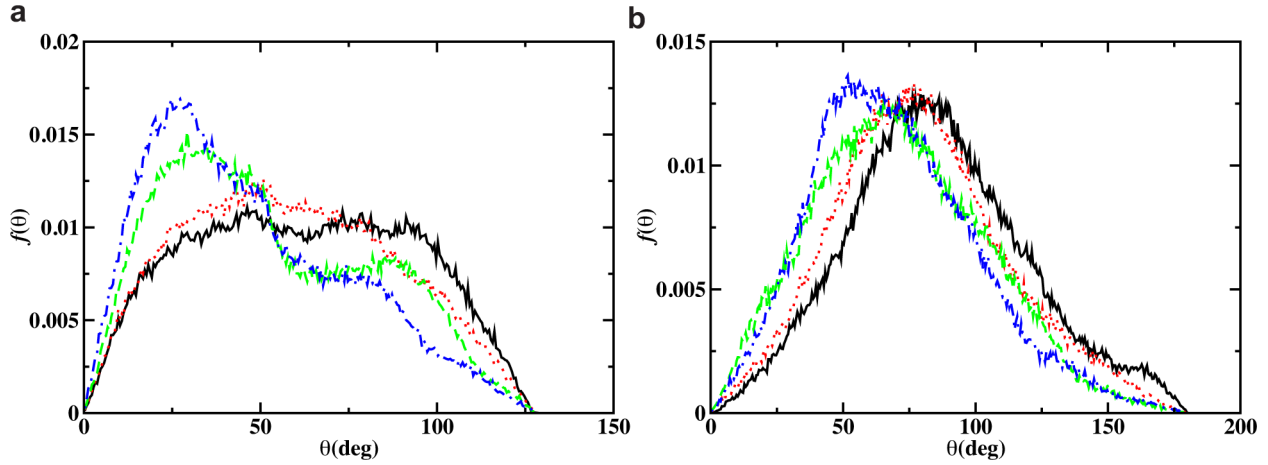

Figure 10. Orientational analysis for water molecules in the apical region: (a) distribution of the angle between the OU−OW vector and OW−HW vector for the hydrogen site closer to OU; (b) distribution of the angle between OU−OW with water dipole moment. The colors have the same meaning as those in Figure 9.

studies by Nichols et al.[93] suggest that the coordination number reported by Soderholm et al.[92] is too small; we speculate that their results do not take into account the water molecules in the apical region. The broadness of the second peak is in part because it includes water molecules of the first solvation shell in the apical region of the uranyl ion. As observed in the case of the first solvation shell, the second solvation shell for the UU−HW RDF extends further out than the UU−OW RDF, but the separation of these peaks is not as clear as in the case of the first solvation shell. This indicates significantly diminished structural ordering in the second solvation shell.

The sharpness of the first peak suggests that there is a very strong structural order in the first solvation shell of the uranyl ion. This structural ordering probably makes the biggest contribution to the entropy of hydration of the uranyl ion. However, UU−OW and OU−OW RDFs show the existence of almost five solvation shells with significantly diminished peak heights with increasing UU−OW and OU−OW separation. This is in contrast with positively charged monovalent ions, which exhibit almost no solvation structure beyond the second solvation shell.[58]

The structural rigidity of the first and second solvation shells is examined by looking at the distribution of the angle that the water dipole moment vector (**p**) makes with the UU−OW vector (θ) and of the tilt angle that the water plane normal (**n**) makes with the UU−OU vector (ϕ), as shown in Figure 9. In the first solvation shell, we find that the UU−OW vector is almost collinear with **p** for all water models except TIP5P. In the case of TIP5P, the distribution peaks at 40° instead of ∼10° for the other models. This is a direct consequence of positive charge and dipole interaction, where the dipole pointing away is energetically more favorable (see CONF1 and CONF2 energetics in Figure 7). In contrast to the θ distribution, the ϕ distribution is rather broad with symmetric peaks at ∼50 and 130°. Furthermore, the region defined by $50° \leq \phi \leq 130°$ is quite accessible. The ϕ distribution shows that hydrogen atoms of the water molecules mainly lie above and below the equatorial plane with very small probability of finding them in the equatorial plane. For TIP4P and SPC/Fw models, there is an additional peak at 90°degrees. Thus, although RDFs and NIs point to a very similar arrangement of all four water models, the θ and ϕ distributions show that there are small differences in the way in which water orders. This is mainly due to the flexibility of the SPC/Fw model and quite different arrangement of point charges in the case of the TIP5P water model. Frick et al.[94] also computed the orientational distribution of water molecules in the first solvation shell. Their representative snapshots suggest that water molecules adopt conformations similar to that observed in the present study. The tilt angle distribution reported by Frick et al.[94] is offset by 90° relative to our distribution most likely due to differences in the definition of tilt angle. For water molecules in the second solvation shell, the θ and ϕ distributions show little variation among the different water models. The θ distribution is much broader than the first solvation shell and peaks at around 50°, while the ϕ distribution has a single peak at 90°. This suggests that water molecules in the second solvation shell have much more mobility than those in the first solvation shell.

There has been significant interest in the nature of bonding of water molecules in the meso shell with the apical oxygens of uranyl ion.[12,77,93,95] An early exploratory work by Guilbaud and Wipff[95] examined the effect of different charge distributions on uranyl coordination. They found that there is strong hydrogen bonding between apical oxygens and water molecules when an unphysically large charge of +6 is placed on the uranium atom. The hydrogen bonding interactions become weaker as the charge is reduced to +4, and disappear for a charge of +3, as evidenced by the OU−OW and OU−HW RDFs.[95] Hagberg et al.[12] found evidence for very weak to almost no hydrogen bonding in the apical region. The lack of hydrogen bonding was further corroborated by density functional calculations.[77] However, CPMD calculations by Nichols et al.[93] state that nearly half the water molecules in the apical region oriented such that hydrogen atoms point to apical oxygen, suggesting the presence of hydrogen bonding.

To analyze orientational ordering in the context of possible hydrogen bonding in the apical region, we plot characteristic angle distributions in Figure 10. The angles are defined by the OU−OW vector with the OW−HW vector (for the hydrogen atom closest to OU) and **p**. Thus, an angle of 180° would be the result of the OW−HW vector pointing directly at the OU site in the first case, and both hydrogen atoms pointing at the OU site in the second case. In the case of the OW−HW bond vector, we find that hydrogen atoms favor an orientation where they are pointing away from the apical oxygen. This can also be confirmed by the OU−OW and OU−HW RDFs in Figure 8.

dx.doi.org/10.1021/jp3028275 | J. Phys. Chem. B 2012, 116, 10885−10897

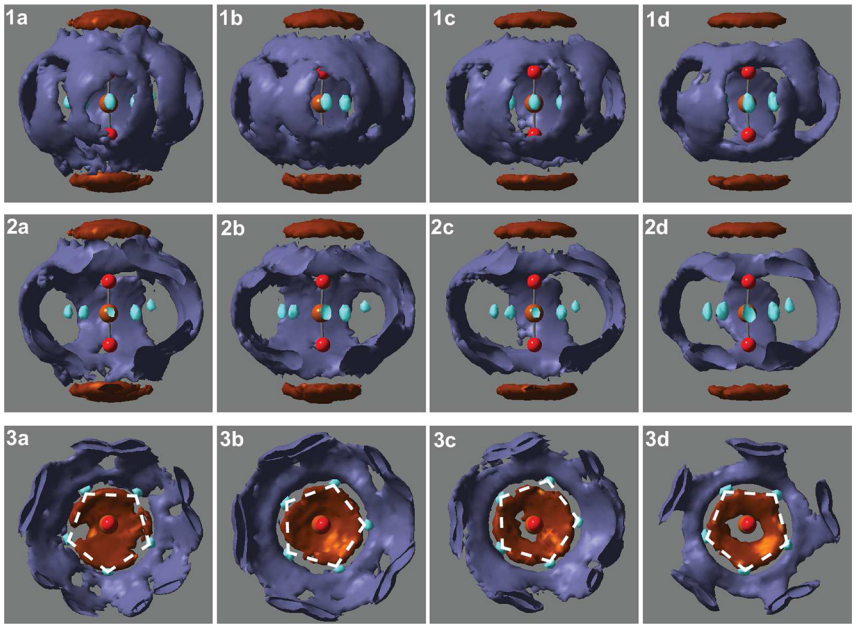

Figure 11. Spatial distribution functions showing most likely positions of water molecules in the first, meso, and second solvation shells of uranyl ion. Subfigure labels 1, 2, and 3 show the front, front section, and top section views, respectively, of SDFs, while labels a, b, c, and d show results for SPC/Fw, TIP3P, TIP4P, and TIP5P, respectively. The cyan, maroon, and purple surfaces show the most likely position water molecules in the first, meso, and second solvation shells, respectively. The white dashed regular pentagons are guides to the eye.

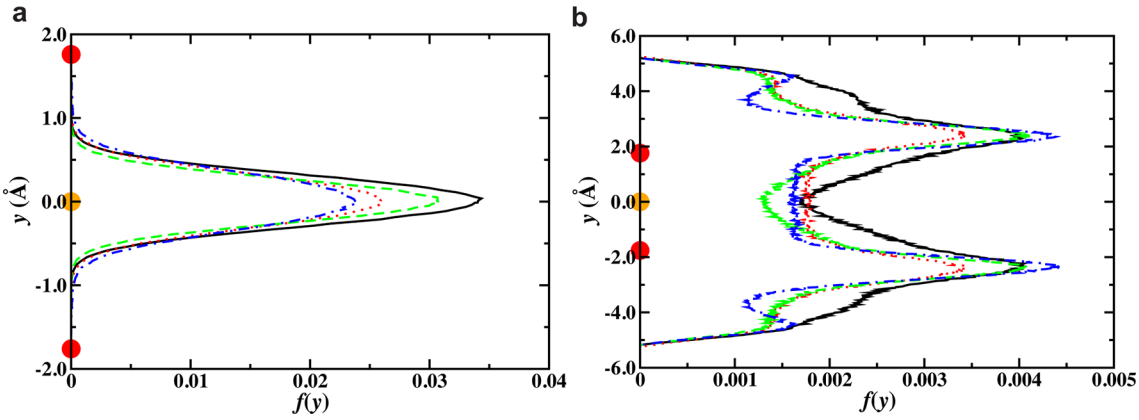

Figure 12. Distribution of the *y*-coordinate of the OW site in the uranyl frame of reference (see Figure 2). Parts a and b show the data for the first and second solvation shells for the UU−OW RDF. The line colors have their usual meaning. The orange and red filled circles represent the location of UU and OU sites for a uranyl in a linear configuration, respectively.

This orientation is more pronounced in the case of TIP4P and TIP5P than the other two water models. The **p** angle distribution shows a peak in the range of 50−90° for different models. This again suggests a lack of any specific hydrogen bonding in the apical region.

To glean three-dimensional information about water molecules around the uranyl ion, SDFs of water molecules in the first and second solvation shells are shown in Figure 11. The SDF presents an isosurface which encapsulates regions of highest probability for finding solvent molecules around a central molecule/ion. Thus, a 50% isosurface will show regions corresponding to 50% of the total probability of finding solvent molecules, while a 100% isosurface will include all regions that have any probability of finding solvent molecules. Figure 11 shows the front, front section, and top section views of SDFs for the most likely positions of water molecules in the first, meso, and second solvation shells for different water models. The shown isosurfaces correspond to 75, 50, and 50% of the total probability density for the first, meso, and second solvation shells, respectively. For the first solvation shell, it is evident that water molecules prefer the equatorial plane (see Figure 12) in contrast to bare uranyl results where water molecules were found to be above and below the equatorial plane. These water molecules are found at the vertices of a regular pentagon. In the case of the second solvation shell, there is a cavity due to the excluded volume of water molecules in the first shell. The SDFs for the second shell suggest that water molecules are hydrogen bonded to the water molecules in the first shell. Furthermore, the presence of troughs along the edges of the pentagon in the SDFs suggest a dynamic equilibrium where second shell water molecules can hydrogen bond with water molecules on either side in the first solvation shell. The *y* distribution for the second solvation shell in the UU−OW RDF shows peaks at approximately 2.2 Å (Figure 12). Thus, there is higher probability of finding water molecules in the region around the apical oxygens than in the equatorial

dx.doi.org/10.1021/jp3028275 | J. Phys. Chem. B 2012, 116, 10885−10897

plane. There are very minor structural differences in the first and second solvation shells for different water models. For the meso shell, however, there are small differences among the water models. The top sections in Figure 11 show that there is a diminished probability of finding water molecules directly above the apical oxygens for TIP4P and TIP5P models.

CONCLUSIONS

Our work shows that many body solvation effects are non-negligible in the case of aqueous ionic systems. The binding energy at the global minimum in UO_2^{2+}/water PES reduces by approximately 35−40% upon solvating uranyl ion relative to an unsolvated "bare" ion. The traditional method of using the bare UO_2^{2+}/water PES is not suitable for generating force fields for condensed phase systems, as it greatly overestimates the binding strength of uranyl ion and water. Simulations based on bare uranyl/water PES overestimate hydration free energies and predict liquid structure which is inconsistent with available experimental data. To develop a force field that represents effective uranyl/water interaction in the condensed phase, it is necessary to incorporate many body solvation effects by solvating the uranyl ion with four water molecules in the equatorial plane when generating the PES. Simulations based on the solvated PES predict correct coordination numbers and hydration free energies. Additionally, we provide a three-dimensional picture of the first and second water solvation shells around the uranyl ion. In the first solvation shell, water molecules are arranged in the equatorial plane at the vertices of a regular pentagon, while in the second solvation shell water molecules are arranged in two annular rings centered near apical oxygens and are connected with longitudinal lobes.

ASSOCIATED CONTENT

Supporting Information

The coordinates for the solvated uranyl complexes are provided in the xyz file. The spatial distribution function for the bare uranyl case and details of soft core potential and surface potential calculations are provided in the PDF file. This material is available free of charge via the Internet at http://pubs.acs.org.

AUTHOR INFORMATION

Corresponding Author

*E-mail: ed@nd.edu.

Notes

The authors declare no competing financial interest.

ACKNOWLEDGMENTS

This material is based upon work supported as part of the Materials Science of Actinides, an Energy Frontier Research Center funded by the U.S. Department of Energy, Office of Science, Office of Basic Energy Sciences under Award Number DE-SC0001089. This research used resources of the National Energy Research Scientific Computing Center, which is supported by the Office of Science of the U.S. Department of Energy under Contract No. DE-AC02-05CH11231. Part of the computational resources were provided by University of Notre Dame Center for Research Computing. We thank Yizhak Marcus for providing clarification about entropy of solvation, Dilip Asthagiri for discussions on proton hydration enthalpies, William Schneider for helpful discussions on the electronic structure calculations, and Andrew Paluch for discussions on hydration free energy calculations.

REFERENCES

(1) Bühl, M.; Wipff, G. *ChemPhysChem* **2011**, *12*, 3095−3105.
(2) Guilbaud, P.; Wipff, G. *J. Mol. Struct.: THEOCHEM* **1996**, *366*, 55−63.
(3) Schuster, P.; Preuss, H.-W. *Chem. Phys. Lett.* **1971**, *11*, 35−37.
(4) Clementi, E.; Popkie, H. *J. Chem. Phys.* **1972**, *57*, 1077−1094.
(5) Sum, A. K.; Sandler, S. I. *Mol. Phys.* **2002**, *100*, 2433−2447.
(6) Ayala, R.; Martinez, J.; Pappalardo, R.; Saint-Martin, H.; Ortega-Blake, I.; Marcos, E. *J. Chem. Phys.* **2002**, *117*, 10512−10524.
(7) Spangberg, D.; Hermansson, K. *J. Chem. Phys.* **2004**, *120*, 4829−4843.
(8) Inada, Y.; Mohammed, A. M.; Loeffler, H. H.; Rode, B. M. *J. Phys. Chem. A* **2002**, *106*, 6783−6791.
(9) Jeziorska, M.; Cencek, W.; Patkowski, K.; Jeziorski, B.; Szalewicz, K. *J. Chem. Phys.* **2007**, *127*, 124303.
(10) Szalewicz, K.; Leforestier, C.; van der Avoird, A. *Chem. Phys. Lett.* **2009**, *482*, 1−14.
(11) Rowley, R. L.; Tracy, C. M.; Pakkanen, T. A. *J. Chem. Phys.* **2006**, *125*, 154302.
(12) Hagberg, D.; Karlstrom, G.; Roos, B.; Gagliardi, L. *J. Am. Chem. Soc.* **2005**, *127*, 14250−14256.
(13) Roos, B. O.; Andersson, K.; Fülscher, M. P.; Malmqvist, P.-A.; Serrano-Andrés, L.; Pierloot, K.; Merchán, M. *Adv. Chem. Phys.*; John Wiley & Sons, Inc.: 2007; pp 219−331.
(14) Hagberg, D.; Bednarz, E.; Edeistein, N. M.; Gagliardi, L. *J. Am. Chem. Soc.* **2007**, *129*, 14136−14137.
(15) Réal, F.; Trumm, M.; Vallet, V.; Schimmelpfennig, B.; Masella, M.; Flament, J.-P. *J. Phys. Chem. B* **2010**, *114*, 15913−15924.
(16) Beuchat, C.; Hagberg, D.; Spezia, R.; Gagliardi, L. *J. Phys. Chem. B* **2010**, *114*, 15590−15597.
(17) Atta-Fynn, R.; Bylaska, E. J.; Schenter, G. K.; de Jong, W. A. *J. Phys. Chem. A* **2011**, *115*, 4665−4677.
(18) Berendsen, H. J. C.; Grigera, J. R.; Straatsma, T. P. *J. Phys. Chem.* **1987**, *91*, 6269−6271.
(19) Wu, Y.; Tepper, H. L.; Voth, G. A. *J. Chem. Phys.* **2006**, *124*, 024503.
(20) Jorgensen, W. L.; Chandrasekhar, J.; Madura, J. D.; Impey, R. W.; Klein, M. L. *J. Chem. Phys.* **1983**, *79*, 926−935.
(21) Mahoney, M. W.; Jorgensen, W. L. *J. Chem. Phys.* **2000**, *112*, 8910−8922.
(22) Werner, H.-J.; Knowles, P. J.; Manby, F. R.; Schütz, M.; Celani, P.; Knizia, G.; Korona, T.; Lindh, R.; Mistrushenkov, A.; Rauhut, G.; et al. *MOLPRO*, version 2008.1, a package of ab initio programs; 2008; see http://www.molpro.net.
(23) Frisch, M. J.; Trucks, G. W.; Schegel, H. B.; Scuseria, G. E.; Robb, M. A.; Cheeseman, J. R.; Scalmani, G.; Barone, V.; Mennucci, B.; Petersson, G. A.; et al. *Gaussian 09*, revision B.1; Gaussian, Inc.: Wallingford, CT, 2009.
(24) Küchle, W.; Dolg, M.; Stoll, H.; Preuss, H. *J. Chem. Phys.* **1994**, *100*, 7535−7542.
(25) Cao, X.; Dolg, M.; Stoll, H. *J. Chem. Phys.* **2003**, *118*, 487−496.
(26) Cao, X.; Dolg, M. *J. Mol. Struct.: THEOCHEM* **2004**, *673*, 203−209.
(27) Dunning, T. H. *J. Chem. Phys.* **1989**, *90*, 1007−1023.
(28) Peterson, K. A.; Dunning, T. H. *J. Chem. Phys.* **2002**, *117*, 10548−10560.
(29) Feller, D. *J. Comput. Chem.* **1996**, *17*, 1571−1586.
(30) Schuchardt, K. L.; Didier, B. T.; Elsethagen, T.; Sun, L.; Gurumoorthi, V.; Chase, J.; Li, J.; Windus, T. L. *J. Chem. Inf. Model.* **2007**, *47*, 1045−1052.
(31) http://www.theochem.uni-stuttgart.de/pseudopotentials/clickpse.html.
(32) Møller, C.; Plesset, M. S. *Phys. Rev.* **1934**, *46*, 618−622.
(33) Boys, S.; Bernardi, F. *Mol. Phys.* **1970**, *19*, 553−566.
(34) van Duijneveldt, F. B.; van Duijneveldt-van de Rijdt, J. G. C. M.; van Lenthe, J. H. *Chem. Rev.* **1994**, *94*, 1873−1885.

(35) Singh, U. C.; Kollman, P. A. *J. Comput. Chem.* **1984**, *5*, 129−145.
(36) Besler, B. H.; Merz, K. M.; Kollman, P. A. *J. Comput. Chem.* **1990**, *11*, 431−439.
(37) Rappe, A. K.; Casewit, C. J.; Colwell, K. S.; Goddard, W. A.; Skiff, W. M. *J. Am. Chem. Soc.* **1992**, *114*, 10024−10035.
(38) Scalmani, G.; Frisch, M. J. *J. Chem. Phys.* **2010**, *132*, 114110.
(39) Stephens, P. J.; Devlin, F. J.; Chabalowski, C. F.; Frisch, M. J. *J. Phys. Chem.* **1994**, *98*, 11623−11627.
(40) Frenkel, D.; Smit, B. *Understanding Molecular Simulation From Algorithms to Applications*; Academic Press: New York, 2002.
(41) Ewald, P. *Ann. Phys.* **1921**, *64*, 253−287.
(42) Allen, M. P.; Tildesley, D. J. *Computer Simulation of Liquids*; Clarendon Press: Oxford, U.K., 1987.
(43) Vlugt, T. J. H.; Martin, M. G.; Smit, B.; Siepmann, J. I.; Krishna, R. *Mol. Phys.* **1998**, *94*, 727−733.
(44) Shah, J. K.; Maginn, E. J. *J. Chem. Phys.* **2011**, *135*, 134121.
(45) Macedonia, M. D.; Maginn, E. J. *Mol. Phys.* **1999**, *96*, 1375−1390.
(46) Dennington, R.; Keith, T.; Millam, J. *GaussView*, version 5; Semichem Inc.: Shawnee Mission, KS, 2009.
(47) Hess, B.; Kutzner, C.; van der Spoel, D.; Lindahl, E. *J. Theor. Comput. Chem.* **2008**, *4*, 435−447.
(48) Van Der Spoel, D.; Lindahl, E.; Hess, B.; Groenhof, G.; Mark, A. E.; Berendsen, H. J. C. *J. Comput. Chem.* **2005**, *26*, 1701−1718.
(49) H, C.; Bennett. *J. Comput. Phys.* **1976**, *22*, 245−268.
(50) Warren, G. L.; Patel, S. *J. Chem. Phys.* **2007**, *127*, 064509.
(51) Miyamoto, S.; Kollman, P. A. *J. Comput. Chem.* **1992**, *13*, 952−962.
(52) Darden, T.; York, D.; Pedersen, L. *J. Chem. Phys.* **1993**, *98*, 10089−10092.
(53) Essmann, U.; Perera, L.; Berkowitz, M. L.; Darden, T.; Lee, H.; Pedersen, L. G. *J. Chem. Phys.* **1995**, *103*, 8577−8593.
(54) Vangunsteren, W. F.; Berendsen, H. J. C. *Mol. Phys.* **1982**, *45*, 637−647.
(55) Parrinello, M.; Rahman, A. *J. Appl. Phys.* **1981**, *52*, 7182−7190.
(56) Nosé, S.; Klein, M. *Mol. Phys.* **1983**, *50*, 1055−1076.
(57) Horinek, D.; Mamatkulov, S. I.; Netz, R. R. *J. Chem. Phys.* **2009**, *130*, 124507.
(58) Warren, G. L.; Patel, S. *J. Chem. Phys.* **2007**, *127*, 064509.
(59) Darden, T.; Pearlman, D.; Pedersen, L. G. *J. Chem. Phys.* **1998**, *109*, 10921.
(60) Hummer, G.; Pratt, L. R.; García, A. E. *J. Chem. Phys.* **1997**, *107*, 9275.
(61) Kastenholz, M. a.; Hünenberger, P. H. *J. Chem. Phys.* **2006**, *124*, 224501.
(62) Hummer, G.; Pratt, L. R.; Garca, A. E. *J. Phys. Chem.* **1996**, *100*, 1206−1215.
(63) Adamo, C.; Barone, V. *J. Chem. Phys.* **1999**, *110*, 6158−6170.
(64) Raghavachari, K.; Trucks, G. W.; Pople, J. A.; Head-Gordon, M. *Chem. Phys. Lett.* **1989**, *157*, 479−483.
(65) Vydrov, O. A.; Scuseria, G. E. *J. Chem. Phys.* **2006**, *125*, 234109.
(66) Aberg, M.; Ferri, D.; Glaser, J.; Grenthe, I. *Inorg. Chem.* **1983**, *22*, 3986−3989.
(67) Wahlgren, U.; Moll, H.; Grenthe, I.; Schimmelpfennig, B.; Maron, L.; Vallet, V.; Gropen, O. *J. Phys. Chem. A* **1999**, *103*, 8257−8264.
(68) Sémon, L.; Boehme, C.; Billard, I.; Hennig, C.; Lützenkirchen, K.; Reich, T.; Robberg, A.; Rossini, I.; Wipff, G. *ChemPhysChem* **2001**, *2*, 591−598.
(69) Allen, P. G.; Bucher, J. J.; Shuh, D. K.; Edelstein, N. M.; Reich, T. *Inorg. Chem.* **1997**, *36*, 4676−4683.
(70) Neuefeind, J.; Soderholm, L.; Skanthakumar, S. *J. Phys. Chem. A* **2004**, *108*, 2733−2739.
(71) Bardin, N.; Rubini, P.; Madic, C. *Radiochim. Acta* **1998**, *83*, 189−194.
(72) Marcus, Y. *J. Inorg. Nucl. Chem.* **1975**, *37*, 493−501.
(73) Marcus, Y. *Ion Solvation*; John Wiley and Sons Ltd.: 1985; pp 107−125.
(74) Marcus, Y. *Ion Properties*; Marcel Dekker: 1997.
(75) Shamov, G. A.; Schreckenbach, G. *J. Phys. Chem. A* **2005**, *109*, 10961−10974.
(76) Shamov, G. A.; Schreckenbach, G. *J. Phys. Chem. A* **2006**, *110*, 12072−12072.
(77) Gutowski, K. E.; Dixon, D. A. *J. Phys. Chem. A* **2006**, *110*, 8840−8856.
(78) Gibson, J. K.; Haire, R. G.; Santos, M.; Marçalo, J.; Pires de Matos, A. *J. Phys. Chem. A* **2005**, *109*, 2768−2781.
(79) Halliwell, H. F.; Nyburg, S. C. *Trans. Faraday Soc.* **1963**, *59*, 1126−1140.
(80) Tissandier, M. D.; Cowen, K. A.; Feng, W. Y.; Gundlach, E.; Cohen, M. H.; Earhart, A. D.; Coe, J. V.; Tuttle, T. R. *J. Phys. Chem. A* **1998**, *102*, 7787−7794.
(81) Tuttle, T. R.; Malaxos, S.; Coe, J. V. *J. Phys. Chem. A* **2002**, *106*, 925−932.
(82) Camaioni, D. M.; Schwerdtfeger, C. A. *J. Phys. Chem. A* **2005**, *109*, 10795−10797.
(83) Asthagiri, D.; Pratt, L. R.; Ashbaugh, H. S. *J. Chem. Phys.* **2003**, *119*, 2702−2708.
(84) Lamoureux, G.; Roux, B. *J. Phys. Chem. B* **2006**, *110*, 3308−3322.
(85) Grossfield, A.; Ren, P.; Ponder, J. W. *J. Am. Chem. Soc.* **2003**, *125*, 15671−15682.
(86) Cornehl, H. H.; Heinemann, C.; Marcalo, J.; de Matos, A. P.; Schwarz, H. *Angew. Chem., Int. Ed. Engl.* **1996**, *35*, 891−894.
(87) Hemmingsen, L.; Amara, P.; Ansoborlo, E.; Field, M. J. *J. Phys. Chem. A* **2000**, *104*, 4095−4101.
(88) Clavaguéra-Sarrio, C.; Brenner, V.; Hoyau, S.; Marsden, C. J.; Millié, P.; Dognon, J.-P. *J. Phys. Chem. B* **2003**, *107*, 3051−3060.
(89) Wahlgren, U.; Moll, H.; Grenthe, I.; Schimmelpfennig, B.; Maron, L.; Vallet, V.; Gropen, O. *J. Phys. Chem. A* **1999**, *103*, 8257−8264.
(90) Ankudinov, A. L.; Conradson, S. D.; Mustre de Leon, J.; Rehr, J. J. *Phys. Rev. B* **1998**, *57*, 7518−7525.
(91) Conradson, S. D. *Appl. Spectrosc.* **1998**, *52*, 252A−279A.
(92) Soderholm, L.; Skanthakumar, S.; Neuefeind, J. *Anal. Bioanal. Chem.* **2005**, *383*, 48−55.
(93) Nichols, P.; Bylaska, E. J.; Schenter, G. K.; de Jong, W. *J. Chem. Phys.* **2008**, *128*, 124507.
(94) Frick, R. J.; Hofer, T. S.; Pribil, A. B.; Randolf, B. R.; Rode, B. M. *J. Phys. Chem. A* **2009**, *113*, 12496−12503.
(95) Guilbaud, P.; Wipff, G. *J. Phys. Chem.* **1993**, *97*, 5685−5692.
(96) Martínez, J. M.; Torrico, F.; Pappalardo, R. R.; Sanchez Marcos, E. *J. Phys. Chem. B* **2004**, *108*, 15851−15855.